Acta Pharmaceutica Sinica B 2024;14(10):4544–4559

Chinese Pharmaceutical Association
Institute of Materia Medica, Chinese Academy of Medical Sciences

Acta Pharmaceutica Sinica B

www.elsevier.com/locate/apsb
www.sciencedirect.com

ORIGINAL ARTICLE

Choroid plexus CCL2–CCR2 signaling orchestrates macrophage recruitment and cerebrospinal fluid hypersecretion in hydrocephalus

Qiguang Wang [a], Fei Liu [d], Yue Li [f], Huan Zhang [a], Xin Qi [a], Ke Wu [e], Yi Zhang [f], Shenglan You [f], Wenke Liu [a], Xuhui Hui [a], Hanmei Li [g], Lei Zhu [c,*], Huile Gao [b,*], Jian Cheng [a,*]

[a]*Department of Neurosurgery, West China Hospital, Sichuan University, Chengdu 610041, China*
[b]*Key Laboratory of Drug-Targeting and Drug Delivery System of the Education Ministry, West China School of Pharmacy, Sichuan University, Chengdu 610041, China*
[c]*Institute of Thoracic Oncology, West China Hospital, Sichuan University, Chengdu 610041, China*
[d]*Institutes for Systems Genetics, Frontiers Science Center for Disease-Related Molecular Network, West China Hospital, Sichuan University, Chengdu 610041, China*
[e]*Institute of Rare Diseases, West China Hospital of Sichuan University, Chengdu 610041, China*
[f]*Research Core Facility of West China Hospital, Sichuan University, Chengdu 610041, China*
[g]*Key Laboratory of Coarse Cereal Processing, School of Food and Biological Engineering, Chengdu University, Chengdu 610106, China*

Received 15 March 2024; received in revised form 16 June 2024; accepted 17 June 2024

KEY WORDS

Hydrocephalus;
Macrophages;
CCL2;
CCR2;
Choroid plexus;
Epithelial cells;
Crosstalk;

Abstract The choroid plexus (ChP) serves as the principal origin of cerebrospinal fluid (CSF). CSF hypersecretion due to ChP inflammation has emerged as an important pathogenesis of hydrocephalus recently. Nevertheless, the precise mechanisms of ChP inflammation and the ensuing CSF hypersecretion in hydrocephalus remain ill-defined. In the present study, we elucidate the critical role of macrophages in the pathogenesis of ChP inflammation. Specifically, we identify the chemokine CCL2, released by ChP epithelial cells, recruits $CCR2^{+}$ monocytes to the ChP thereby inciting hydrocephalus pathogenesis. The accumulated ChP macrophages increase the inflammation in ChP epithelial cells through TNF-α/TNFR1/NF-κB signaling cascade, thereby leading to CSF hypersecretion. Strikingly, augmentation of ChP–CCL2 using an adeno-associated

*Corresponding authors.
E-mail addresses: lei_zhu@scu.edu.cn (Lei Zhu), gaohuile@scu.edu.cn (Gao), chengjian@scu.edu.cn (Jian Cheng).

Peer review under the responsibility of Chinese Pharmaceutical Association and Institute of Materia Medica, Chinese Academy of Medical Sciences.

https://doi.org/10.1016/j.apsb.2024.06.020

Cerebrospinal fluid hypersecretion

viral approach (AAV) exacerbates macrophage recruitment, activation, and ventriculomegaly in rat PHH models. Systemic application of Bindarit, a specific CCL2 inhibitor, significantly inhibits ChP macrophage infiltration and activation and reduces CSF secretion rate. Furthermore, the administration of CCR2 antagonist (INCB 3284) reduces ChP macrophage accumulation and ventriculomegaly. This study not only unveils the ChP CCL2−CCR2 signaling in the pathophysiology of hydrocephalus but also unveils Bindarit as a promising therapeutic choice for the management of posthemorrhagic hydrocephalus.

1. Introduction

Intraventricular hemorrhage (IVH), subarachnoid hemorrhage (SAH), and intracerebral hemorrhage (ICH) frequently extend into the ventricular system, leading to posthemorrhagic hydrocephalus (PHH)[1-3]. The severe and persistent elevation of intracranial pressure can lead to brainstem herniation and even fatal outcomes[4]. The precise mechanisms of hydrocephalus remain poorly defined, and novel targeted therapeutic approaches are lacking. Cerebrospinal fluid (CSF) shunting, an empirical "one-size-fits-all" approach, remains the standard treatment of hydrocephalus; however, it carries a high risk of serious complications such as shunt obstruction and infection[4]. Of particular concern, long-term follow-up studies reveal that nearly 40%−45% of patients with shunted hydrocephalus experience serious chronic headaches, depression, dependency on care, and unemployment[5-7]. This highlights the necessity of developing specific pharmacotherapeutic strategies to address hydrocephalus effectively.

The choroid plexus (ChP) secretes >500 cc/day of CSF into brain ventricular spaces[8]. The balance between CSF secretion by the ChP, and its reabsorption through the arachnoid granulations into the cerebral venous system is of utmost significance to ensure CSF homeostasis[9]. CSF hypersecretion has recently been established as a critical mechanism in the pathogenesis of hydrocephalus[3,10-12]. Researchers have discovered that IVH-induced CPE inflammation leads to a significant 3.5-fold increase in CSF secretion, which is associated with upregulated phosphorylation of SPAK−NKCC1 in ChP epithelial cells[3,13]. However, the initial factors responsible for initiating ChP inflammation and the underlying molecular mechanisms in driving CSF hypersecretion remain elusive. To address this knowledge gap, we established PHH rat models and conducted transcriptional profiling to gain insights into the molecular pathology of PHH. The ChP transcriptional profiling suggested significant alterations in leukocyte-mediated immunity and leukocyte migration in PHH. Subsequently, we employed the CIBERSORT algorithm[14,15] and found monocyte-macrophages might play a central role in ChP inflammation.

ChP serves as a critical entry site for pathogens, acts as a checkpoint for peripheral immune cells entry into the central nervous system (CNS), and regulates cytokines and other signaling molecules in the CSF[16,17]. Despite the present study and Robert et al.[18,19] have observed the accumulation of macrophages in the ChP following IVH, the specific molecular mechanisms in driving ChP macrophage activation and recruitment of circulating monocytes to the ChP in PHH remain poorly understood. Therefore, we conducted a comprehensive analysis of enriched pathways. Our findings indicate the interaction between cytokines and their receptors may play a central role in mediating ChP inflammation orchestrated by macrophages. Previous studies have reported chemokines and cytokines in CSF are involved in the accumulation of immune cells at the ChP during various pathological conditions (*e.g.*, IFNγ signaling promoting the monocyte infiltration across the ChP in Alzheimer's disease, CCR6 signaling for Th17 recruitment in experimental autoimmune encephalomyelitis)[16,20]. We then emphasized the analysis of chemokines and their receptors related to macrophages and found chemokine (C−C motif) ligand 2 (CCL2) was one of the leading chemokines that overexpressed in the ChP in hydrocephalus. Notably, CCL2 is known to interact with C−C motif chemokine receptor 2 (CCR2) to modulate monocyte recruitment in several inflammatory diseases[21-24]. However, the involvement of CCL2−CCR2 and macrophages in the ChP of hydrocephalus has not been investigated thus far.

In this study, we identified the pivotal function of chemokine CCL2, which is preferentially released by ChP epithelial cells upon activation by LPS or hemorrhage. This chemokine plays a crucial role in recruiting circulating $CCR2^+$ monocytes to the ChP, resulting in CSF hypersecretion and the formation of hydrocephalus. Furthermore, we have elucidated the underlying mechanisms of ChP epithelial cells and macrophage interaction in the pathogenesis of hydrocephalus. In rat PHH models, targeting CCL2 using Bindarit significantly suppressed ChP macrophage infiltration, CSF secretion, and hydrocephalus formation.

2. Materials and methods

2.1. Animals

Male Sprague−Dawley rats aged 7−9 weeks and weighted 220−250 g were obtained from the Chengdu Dossy Experimental Animals Co., Ltd. (Chengdu, China). The rats were housed in a temperature-controlled room on a 12-h light/12-h dark cycle with a standard rat diet and water ad libitum. All experimental procedures involving animals were in accordance with the Animal Research: Reporting *In Vivo* Experiments (ARRIVE) Guidelines 2.0[25], and approved by the Laboratory Animal Welfare and Ethics Committee of West China Hospital of Sichuan University (Approval/accreditation number is 20220921001).

2.2. Cell culture and treatments

We cultured primary ChP epithelial cells from rats according to the previously described method[26]. Briefly, we isolated the brains of rats and then isolated and plated the ChP into freshly prepared sterile dissection media, consisting of 1 × DMEM and 1 × penicillin streptomycin. The tissue was repeatedly cut up in a 1.5 mL sterile EP tube. Then the pieces of ChP tissue were

digested with pancreatin and aspirated repeatedly with a 200-μL pipette. The tissue was then resuspended in a choroid plexus epithelial cells (CPEC) media after centrifugation. CPEC media included 10% fetal bovine serum (FBS), 10,000 units/mL penicillin streptomycin, and 10 ng/mL human EGF in DMEM. The ChP epithelial cells were cultured for 14 days, with the media changed every 2−3 days, and then used for experiments.

The rat macrophage NR8383 cells were purchased from the National Collection of Authenticated Cell Cultures (Beijing, China). The cells were incubated at 37 °C in DMEM supplemented with 1% penicillin-streptomycin and 10% FBS under 5% CO_2 atmosphere.

To stimulate the inflammatory response, the primary ChP epithelial cells and NR8383 cells were treated with LPS (100 ng/mL) (cat: L8880, Solaribio, Beijing, China). To inhibit TNF-α receptors, the ChP epithelial cells were treated with R7050 (cat: HY-110203, MCE, New Jersey, USA). To block TNF-α signaling, the Anti-TNFα antibody (cat:80045-RP02, Sino Biological, Beijing, China) was added to the NR8383-derived conditional medium and cultured with ChP epithelial cells. To explore the possible mechanism by which macrophage-derived TNF-α affects the inflammation and CSF secretion, the ChP epithelial cells were treated with recombinant rat TNF-α (cat: 400-14-5, Peprotech, New Jersey, USA). To block NF-κB signaling, the ChP epithelial cells were treated with Bay117082 (cat: HY-13453, MCE, New Jersey, USA). To inhibit the LPS indued CCL2 production in ChP epithelial cells, the Bindarit (cat: HY-B0498, MCE, New Jersey, USA) was used.

2.3. Transcriptome sequencing of ChP

The rats in both shame and IVH groups at 48 h post-surgery underwent cranial MRI scans. The ChP of lateral ventricles was dissected in rats with obviously enlarged ventricles on cranial MRI. Total RNA from the ChP was isolated using TRIzol reagent (Invitrogen, USA) and then subjected to quantification and purity assessment using a NanoDrop ND-1000 instrument (NanoDrop, USA). RNA integrity was assessed using an Agilent 2100 instrument, with a RIN >7.0 considered as the qualified standard. Subsequently, the qualified RNA samples were submitted to Novogene Bioinformatics Technology Co., Ltd. (Tianjin, China), for library preparation and sequencing using the Illumina NovaSeq 6000. Then the fragments per kilobase per million reads (FPKM) were used to ascertain the expression levels of the transcripts. The thresholds of significantly different expression were $P < 0.05$ and FPKM $\geq$1.8. Further studies using the GO and KEGG databases were conducted to explore the functions and biological pathways in which the differentially expressed genes were involved.

2.4. Transwell assay

The NR8383 cells and primary ChP epithelial cells were resuspended using serum-free high-sugar DMEM medium and subsequently cultured in a Transwell chamber. After the cells adhered to the chamber walls and cultured for 24 h, different treatments were introduced based on the previous grouping. After a 24-h incubation period. The samples were collected and the chambers were fixed using 4% paraformaldehyde solution for 15 min. Then they were washed twice with PBS. Subsequently, the chambers underwent staining with crystal violet for a minimum of 20 min. The cells on the inner membrane of the chamber were removed. Finally, the images of the outer membrane of the chamber were obtained using a positive fluorescence microscope.

2.5. Posthemorrhagic hydrocephalus (PHH) models

Following successful anesthesia induction, the rats were meticulously positioned within a precisely aligned stereotaxic frame. A cranial burr hole, 1 mm in diameter, was meticulously drilled at precise coordinates (0.6 mm posterior and 1.6 mm lateral to bregma), with utmost care to maintain accuracy. After the surgical procedure, the operative site was diligently shielded using sterile gauze to prevent contamination. Subsequently, the right femoral artery was meticulously dissected using sharp techniques, and a catheter was carefully inserted to facilitate the collection of blood samples. To introduce the blood sample into the brain ventricle, a 29-gauge needle was gently inserted to a depth of 4.5 mm from the dura mater. Gradual infusion of 200 μL of nonheparinized arterial blood ensued, meticulously maintained at a constant rate of 14 μL/min. Vigilance was exercised to avoid any potential backflow, with the needle being maintained *in situ* for an additional duration of 10 min. After this critical period, the incision site was meticulously sutured to promote appropriate wound healing.

2.6. Quantification of the CSF secretion rate

The procedure for measuring the rate of CSF secretion was described by Karimy et al.[3] Firstly, rats were anesthetized and placed on a stereotactic apparatus. A 1 mm cranial burr hole was then drilled on the left ventricle at coordinates 0.6 mm posterior and 1.6 mm lateral to bregma. The burr hole was used to secure a ventricular infusion tube, inserted to a depth of 4.5 mm. Then the rats' head position was changed to expose the occiput. Suboccipital muscles were dissected to expose the atlantooccipital ligament. To reach the fourth ventricle, a 29-gauge needle was punctured through the atlantooccipital ligament after dissection of the suboccipital muscles. By occluding the aqueduct Sylvius with 100 μL of sterile molecular-grade mineral oil (Sigma−Aldrich, USA), CSF flow from the third ventricle to the fourth ventricle was prevented, establishing a closed CSF circulation in the lateral ventricles. A straight PE tube (OD: 0.5 mm, ID: 1 mm, length: 20 cm) was then connected flush and perpendicular to the fixed tube while the rat's head remained in the same position with the nose pointing downward after a gentle 90° rotation using the ear bars. To calculate the volume of CSF collected over 40 min, formula $V\ (\mathrm{mm}^3) = \pi \cdot r^2 \cdot d$ was employed, where "r" represents the radius of the PE tube and "d" indicates the distance that CSF traveled within the tube. Subsequently, the rate of CSF formation (μL/min) was calculated.

2.7. CSF collection

After 48 h of PHH model surgery, the anesthetized rats were secured in a stereotactic apparatus. Then the rat's head was rotated 90° on the ear-bars, facing downward, and the suboccipital muscles were dissected to access the cisterna magna and expose the atlantooccipital ligament. Then the ligament was punctured using a 27G needle attached to a 1 mL syringe and then inserted into the cisterna magna. Then approximately 100 μL cerebrospinal fluid (CSF) was collected. After a centrifugation of 1000 rpm (Thermo Fisher, Waltham Mass, USA) for 3 min. The samples were stored at −80 °C for further analysis using the Rat Cytokine Array/Chemokine Array (Neobioscience, Shen Zhen, China).

2.8. Cytokine/chemokine/protein measurements

For the measurement of cytokine levels (Rat CCL2, TNF-α, and IL-1β) in the CSF, inflammation cytokine assay kits from Neobioscience (Shen Zhen, China) were used, following the manufacturer's guidelines.

2.9. Quantitative PCR analysis

Total RNA from the cells and ChP samples was extracted using TRIzol reagent purchased from Thermo Fisher Scientific (Waltham, MA, USA). Subsequently, cDNA was synthesized using a reverse transcription kit (Vazyme, Nanjing, China). To amplify the target mRNAs, quantitative PCR was performed. The primer sets used for the targeted genes can be found in Supporting Information Table S1. Finally, the expression of these targeted genes was evaluated and normalized to GAPDH.

2.10. Drug administration

Bindarit (cat: HY-B0498) and INCB3284 (cat: HY-15450A) were purchased from MedChemExpress (MCE, New Jersey, USA). Bindarit was used to block CCL2 synthesis and INCB3284 was applied to inhibit the combination between CCL2 and CCR2. Bindarit and INCB3284 were dissolved in DMSO and diluted with corn oil. The control rats were administrated with vehicle (10% DMSO in corn oil). The rats received intraperitoneal injections of Bindarit (30 mg/kg) or INCB3284 (1 mg/kg) every 12 h starting 12 h before IVH and continuing until 36 h after IVH.

2.11. Magnetic resonance imaging (MRI)

The rats were imaged using Bruker BioSpec small animal 7T MRI (Bruker, Germany) at 48 h after IVH under anesthesia by isoflurane. Monitoring of breathing rate and heart rate provided insight into anesthesia depth. Axial T2 images were acquired and the volume of lateral ventricles was calculated using 3D-Slicer software (NIH, MD, USA).

2.12. Western blot analysis

After different treatments, the cells and ChP tissues were collected. For the Western blot, we utilized the following primary antibodies: CD68 (Proteintech, 28058-1-AP), IBA-1 (Proteintech, 10904-1-AP), TNFR1 (Proteintech, 21574-1-AP), β-actin (Abcam, ab8227), CCL2 (Abcam, ab7202), p-NKCC1 (Sigma, ABS1004), NKCC1 (Abcam, ab303518), NF-κB(CST,8242), pNF-κB (CST, 3033), iNOS (Abcam, ab178945). The immunoreactive bands' relative densities were standardized against those of β-actin and subsequently subjected to analysis *via* ImageJ.

2.13. Immunofluorescence staining

Brain tissue immunofluorescence staining was conducted on fixed frozen sections, following established protocols. Rats with different treatments were anesthetized using intraperitoneal pentobarbital (40 mg/kg) and then perfused with 4% paraformaldehyde upon reaching deep anesthesia. The brains were quickly removed and fixed in 4% paraformaldehyde (PFA; in PBS) overnight at 4 °C. The samples were washed using PBS and subsequently cryoprotected in a 30% sucrose-PBS solution. Following this, they were immersed in NEG50 freezing medium from Thermo Fisher Scientific (Waltham, MA, USA), and 10-mm-thick cryosections were carefully prepared. Then the frozen sections were washed with PBS three times and blocked with a blocking buffer (ab126587, Abcam) for 30 min at the RT. Next, the sections were stained with primary antibodies at 4 °C overnight. We utilized the following primary antibodies: CD68 (Proteintech,28058-1-AP), IBA-1 (Proteintech; Abcam, 10904-1-AP; ab283319), CCR2 (Abcam, ab273050), Ki67 (Abcam, ab15580), TNFR1 (Proteintech, 21574-1-AP), TNFR2 (Proteintech, 19272-1-AP), pNKCC1 (Sigma, ABS1004), TNF-α (Abcam, ab307164), NF-κB (CST, 8242), ZO-1 (Abcam, ab221547), TTR (Abcam, ab271132). On the following day, the brain sections were washed three times in PBS and incubated for 1 h at RT with secondary antibodies: goat anti-rabbit Alexa 488-conjugated IgG (Jackson,111-545-003), goat anti-mouse Alexa 550-conjugated IgG (Jackson,115-025-003) and goat anti-rabbit Alexa 550-conjugated IgG (Jackson, 111-025-003). Then the sections were stained with DAPI (Abcam, ab228549) after washing 3 times in PBS at RT. At last, sections were mounted with an anti-fade fluorescence mounting medium (Abcam, ab104135). The fluorescent images were captured with Vectra Polaris Multispectral Imaging and Whole Slide Scanning (PerkinElmer, MA, USA).

2.14. Statistical analysis

All graphs and statistical analyses were conducted using GraphPad Prism (version 9.0, GraphPad, USA) and mean ± SEM was used to express all values. A minimum of 3 rats per group was included in *in vivo* experiments. We employed the Student's *t*-test between two groups and one-way ANOVA between multiple groups to assess the notable distinctions among the experimental samples. Statistical significance was denoted by $P < 0.05$ as thresholds.

3. Results

3.1. The active ChP macrophages correlate with robust inflammation of the ChP-CSF interface in PHH

Previous studies have established that CSF hypersecretion due to ChP inflammation plays a pivotal role in the pathogenesis of hydrocephalus[3,27]. However, the precise origins of ChP inflammation remain elusive. To obtain a molecular understanding of ChP-mediated acute CSF hypersecretion in PHH, we conducted transcriptome analysis on micro-dissected ChP samples obtained from the lateral ventricles of rats with PHH and control subjects (Fig. 1A and B). Since not all the IVH rat models exhibit hydrocephalus pathology, we conducted RNA transcriptome sequencing in rats with confirmed hydrocephalus formation on magnetic resonance imaging (MRI) following IVH. The differential gene expression observed in the heatmap indicated significant changes in expression levels (Fig. 1C). Further analysis using Gene Ontology term enrichment revealed that the differentially expressed genes (DEGs) were notably associated with leukocyte-mediated immunity and leukocyte migration (Fig. 1D). Next, to assess the presence of infiltrating immune cells in the ChP of PHH, we employed the CIBERSORTS algorithm for immune-related evaluations. Our findings demonstrated the infiltration of monocytes at ChP, hinting at their potential role in PHH (Fig. 1E and F; Supporting Information Figs. S1A and S1B). Using immunofluorescence and Western blot, we observed a significant accumulation of IBA1$^+$ macrophages at the ChP following IVH (Fig. 1G−J). These macrophages were primarily localized to the

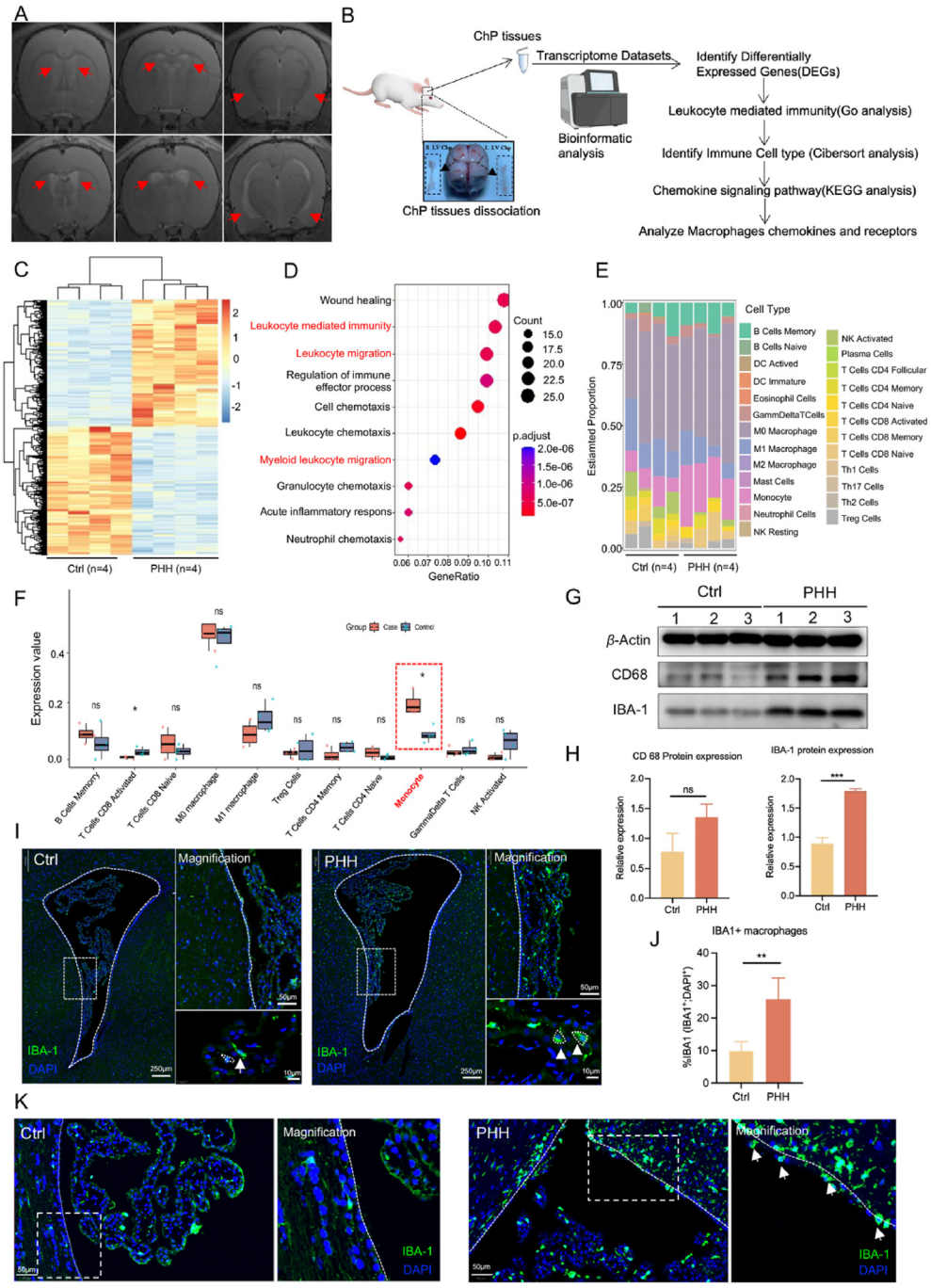

Figure 1 IVH triggers macrophage accumulation and migration in posthemorrhagic hydrocephalus. (A) Representative T2-weighted images depicting enlarged lateral ventricles in hydrocephalus rats. (B) Schematic of integrated transcriptome analysis. (C) Heat map visualizing the differential expressed genes in the ChP between normal and PHH rats. (D) Gene ontology (GO) analysis of biological processes associated with the differentially expressed genes. (E) Inferred composition of 25 immune cell subsets within the ChP of normal and PHH rats. (F) Cibersort algorithm analysis hinted the number of monocytes significantly increased in ChP after IVH. (G) The protein expression of IBA-1 and CD68 in ChP after IVH. (H) Western blot analysis of CD68 and IBA-1 ($n = 3$ animals per condition). (I) Representative fluorescence photos showing immunolabeling for IBA1 (green) positive cells in the ChP after IVH ($n = 5$ animals per condition). Scale bars = 250 μm. (J) Statistical analysis of IBA1+ macrophages. (K) Migration of ChP IBA1+ macrophages (green) observed within the subependymal zone of ctrl and PHH rats. Scale bars = 50 μm. All data were presented as mean ± SD,*$P < 0.05$, **$P < 0.01$ and ***$P < 0.001$ *vs.* control/model.

CSF-facing surface of the ChP and exhibited a distinct morphological shift towards a "round" shape, accompanied by increased circularity (Fig. 1I, white arrow). Additionally, we found significantly increased IBA1$^+$ macrophages in the subependymal zone of PHH rats (Fig. 1K), highlighting ChP macrophage migration in PHH.

Upon recruitment to inflammatory conditions, macrophages undergo activation and differentiation, resulting in the formation

of two distinct subsets known as M1 and M2 in response to various signaling cues. We then performed molecular detection of macrophage markers in the ChP. The QPCR analyses showed M1 markers CD40 and CD86, and the inflammatory genes related to macrophage activation including C3AR and TLR4 significantly increased in PHH ChP (Fig. 2A). But the expression of M2 markers CD36, Arg1, and IL-10 decreased or remained unchanged (Fig. S1C). We further found that PHH increased the population of proliferation Ki67$^+$ cells in lateral ventricle ChP (Fig. 2B and C). In addition, we found increased phagocytic activity of ChP macrophages in PHH after co-staining with the phagocytic marker, CD68 (Fig. 2D and E). These findings suggest IVH triggers the migration, accumulation, and activation of macrophages at the ChP.

In addition, we observed PHH displayed elevated mRNA levels of inflammatory cytokines, such as IL-1α, TNF-α, and IL-1β after IVH (Fig. 2F). Subsequently, we analyzed proinflammatory cytokines, including TNF-α, and IL-1β, in the CSF using ELISA (Fig. S1D). The results indicated that PHH lead to a pro-inflammatory state in both the ChP and CSF. Additionally, we also observed noteworthy alterations in the tight junctions among the ChP epithelial cells after IVH. This is exemplified by a discernible reduction of the tight junction marker, ZO-1 (Fig. S1E).

3.2. *CCL2−CCR2 signaling pathway: A pivotal mechanism responsible for orchestrating macrophage accumulation at the ChP in PHH*

To further investigate the molecular mechanisms underlying macrophage recruitment and accumulation at the ChP in PHH. We conducted a KEGG pathway analysis, which revealed substantial enrichment of pathways associated with cytokine-cytokine receptor interaction and chemokine signaling (Fig. 2G). Hence, we examined the expression profiles of chemokines and receptors involved in macrophage[28] function within the ChP (Fig. 2H and I). Our results demonstrated a significant increase in the expression of CCL7, CCL2, CXCL14, and CCR2 in the ChP of PHH rats ($p < 0.05$). Subsequent validation using QPCR confirmed that CCL2 exhibited the most substantial upregulation among the chemokines studied (Fig. 2J). The elevated CCL2 levels in the inflamed ChP of PHH were further corroborated by Western blot assay analysis (Fig. 2K). We also observed a significant elevation of CSF CCL2 expression using ELISA (Fig. 2L). Furthermore, we observed a positive correlation between ChP CCL2 mRNA expression levels and the lateral ventricle volume ($R^2 = 0.7266$, $n = 6$, $P = 0.0311$) (Fig. 2M). These findings shed light on the potential role of CCL2 in recruiting ChP macrophages in PHH. In addition, our findings revealed a substantial increase in both CCR2 mRNA expression and CCR2$^+$ macrophages in the ChP of PHH cases, as demonstrated by QPCR (Fig. 2N) and immunofluorescent staining (Fig. 2O and P). Given that CCL2 predominantly interacts with CC chemokine receptor 2 (CCR2) to recruit circulating CCR2$^+$ monocytes to inflammation sites[29]. Hence, we speculate that ChP CCL2−CCR2signaling may play an important role in the recruitment and accumulation of ChP macrophages in PHH.

3.3. *Crosstalk between ChP epithelial cells and macrophages in response to inflammatory stimulus in vitro*

Previous studies have demonstrated that CCL2 is predominantly secreted by immune cells in humans and mice[30]. In PHH, epithelial cells constitute the predominant cell category within the choroid plexus[31] (Supporting Information Fig. S2A). Despite the potential contributions of a residual small part of ChP macrophages to the overall CCL2 levels cannot be entirely dismissed, our data underscore the significant role of ChP epithelial cells in elevating CCL2 levels in PHH. In the current study, we found primary ChP epithelial cells abundantly expressed and secreted CCL2 while stimulated with LPS *in vitro*, demonstrated by QPCR (Fig. 3A), Western blot (Fig. 3B), immunofluorescence (Fig. S2B) and ELISA (Fig. S2C). Moreover, *in vivo* experiments using fluorescence *in situ* hybridization (Fig. 3C) revealed increased CCL2 mRNA in ChP epithelial cells, corroborating the findings from *in vitro* studies. Immunohistochemical staining (IHC) of ChP tissue (Fig. 3D and E) further confirmed the expression of CCL2 protein in ChP epithelial cells. Meanwhile, the expression of pNKCC1, an important marker of CSF secretion, increased in ChP of PHH rats (Fig. 3F). These results collectively highlight the significant contribution of ChP epithelial cells to the secretion of CCL2 and its potential implications in PHH. We next asked if primary ChP epithelial cells drive the macrophages' migration and accumulation at the ChP. To test this, we utilized a Transwell co-culture system, where rat primary ChP epithelial cells were cultured in the lower chamber and rat macrophages NR8383 in the upper chamber, and divided them into five groups, including NR8383 cell group, NR8383 and epithelial cells group, NR8383 cells incubated with LPS group, NR8383 and epithelial cells incubated with LPS group, and epithelial and NR8383 cells coculture treated with Bindarit group (Fig. 3I). We found that the presence of ChP epithelial cells in the lower chamber, upon the stimulation of LPS, significantly increased the migration of the NR8383 cells (Fig. 3J). The migration could be suppressed after administration of Bindarit (300 μmol/L) in the lower chamber. Bindarit is a CCL2 inhibitor, we found that Bindarit with a concentration of 300 μmol/L significantly inhibited CCL2 expression in ChP epithelial cells stimulated with LPS at both mRNA and protein levels (Fig. 3G, Fig. S2D and S2E). Hence, we demonstrated that CCL2 expressed by ChP epithelial cells played an important role in recruiting the macrophages.

Subsequently, we investigated the influence of the recruited macrophages on ChP epithelial cells utilizing a co-culture system (Fig. 3K). Notably, p-NKCC1 represents the activated form of $Na^+/K^+/2Cl^-$ cotransporter 1 (NKCC1), which has been established as a key contributor to CSF formation in ChP[8]. Hence, in the present study, we used p-NKCC1 as a crucial marker to reflect CSF secretion in ChP epithelial cells. We cultured NR8383 cells in the lower chamber while primary ChP epithelial cells were placed in the upper chamber, the expression of p-NKCC1 was increased in ChP epithelial cells after stimulated with LPS, as confirmed *via* immunofluorescence (Fig. 3L) and Western blot analysis (Fig. 3H). The findings confirmed macrophages upregulated the expression of pNKCC1 and increased CSF secretion in epithelial cells.

3.4. *Macrophages promote CSF hypersecretion in ChP epithelial cells mainly by activating TNF-α/TNFR1/NF-κB signaling*

We then wanted to know what mediated the interplay between macrophages and ChP epithelial cells during PHH (Fig. 4A). The activated macrophages are known to release substantial quantities of pro-inflammatory cytokines, such as TNF-α, IL-1β, and IL-6[32]. Previous studies have demonstrated that inflammatory cytokines

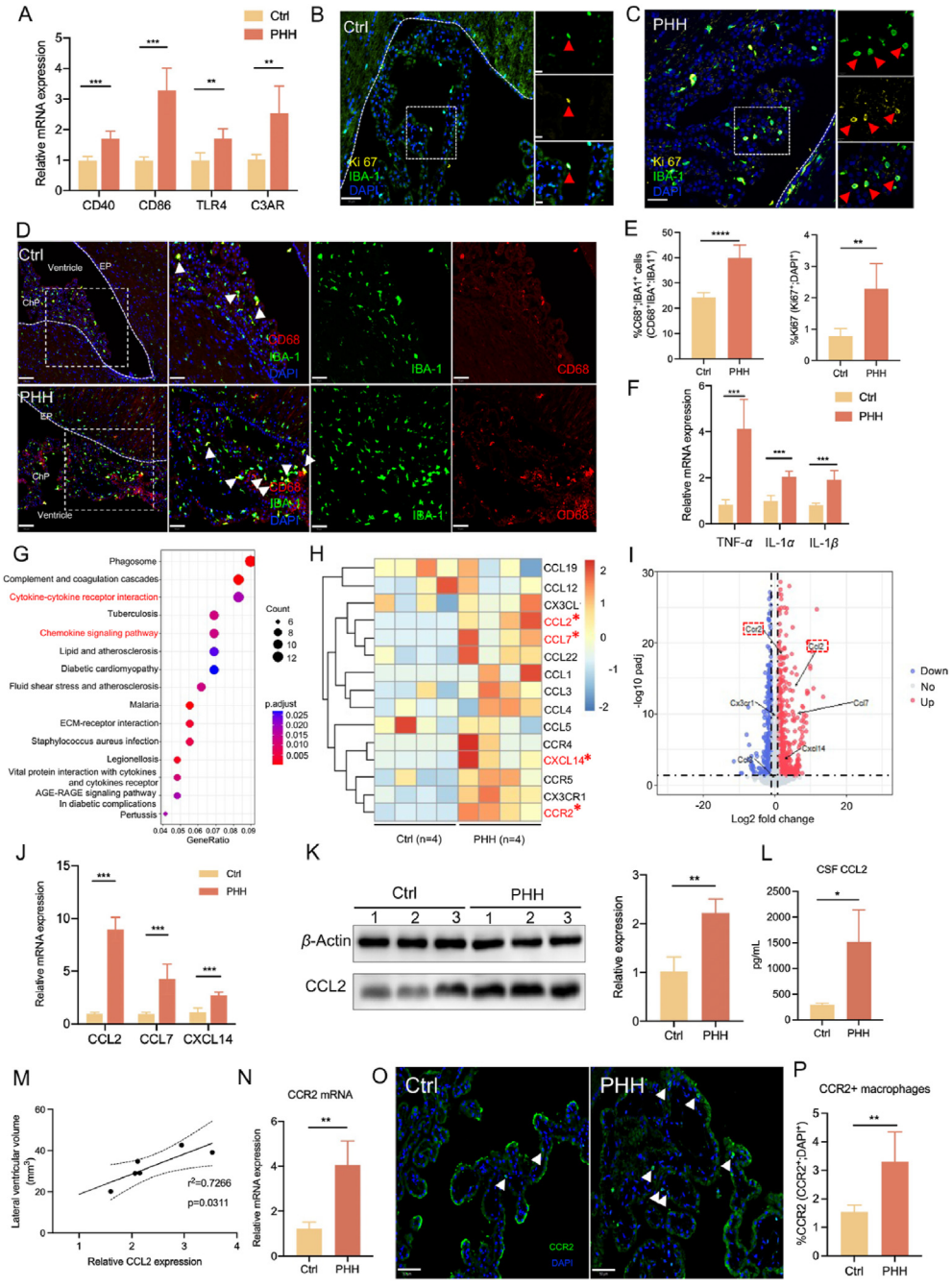

Figure 2 ChP CCL2-CCR2 signaling plays a crucial role in regulating macrophage recruitment and activation. (A) The M1 macrophage markers in ChP of PHH. (B, C) Representative merged and magnified merged and single-channel immunofluorescence of Ki67 (yellow), IBA1 (blue), and DAPI in Ctrl and PHH ($n = 5$ animals per condition). Scale bars = 50 μm. (D) Immunofluorescence of $CD68^+$ (red); $IBA1^+$ (blue) macrophages (white arrow) in Ctrl and PHH ($n = 5$ animals per condition). Scale bars = 50 μm. (E) Quantitative analysis of immunofluorescence findings ($CD68^+$; $Iba1^+$; % of total $Iba1^+$ and % $Ki67^+$ cells). (F) ChP mRNA expression of TNF-α, IL-1α, and IL-1β mRNA in Ctrl or PHH individuals ($n = 5$ animals per condition). (G) KEGG pathway analysis of differentially expressed genes. (H) The chemokines and receptors sequencing related to monocyte-macrophages (*$P < 0.05$). (I) Volcano plots illustrating differentially expressed genes. (J) QPCR analysis of ChP CCL2, CCL7, and CXCL14 expression in Ctrl or PHH rats ($n = 5$ animals per condition). (K) Western blot of ChP CCL2 in Ctrl and PHH rats ($n = 3$ animals per condition). (L) ELISA results of CCL2 expression in CSF ($n = 3$ animals per condition). (M) Correlation between ChP CCL2 expression and ventricular size severity ($r^2 = 0.7266$, $P = 0.0311$). (N) QPCR analysis of ChP CCR2 expression ($n = 5$ animals per condition). (O) Immunofluorescence staining revealing $CCR2^+$ macrophages (white arrow) ($n = 5$ animals per condition), scale bar = 50 μm. (P) Quantitative evaluation of $CCR2^+$ macrophages in all cells. All data were presented as mean ± SD,*$P < 0.05$, **$P < 0.01$ and ***$P < 0.001$ *vs.* control/model.

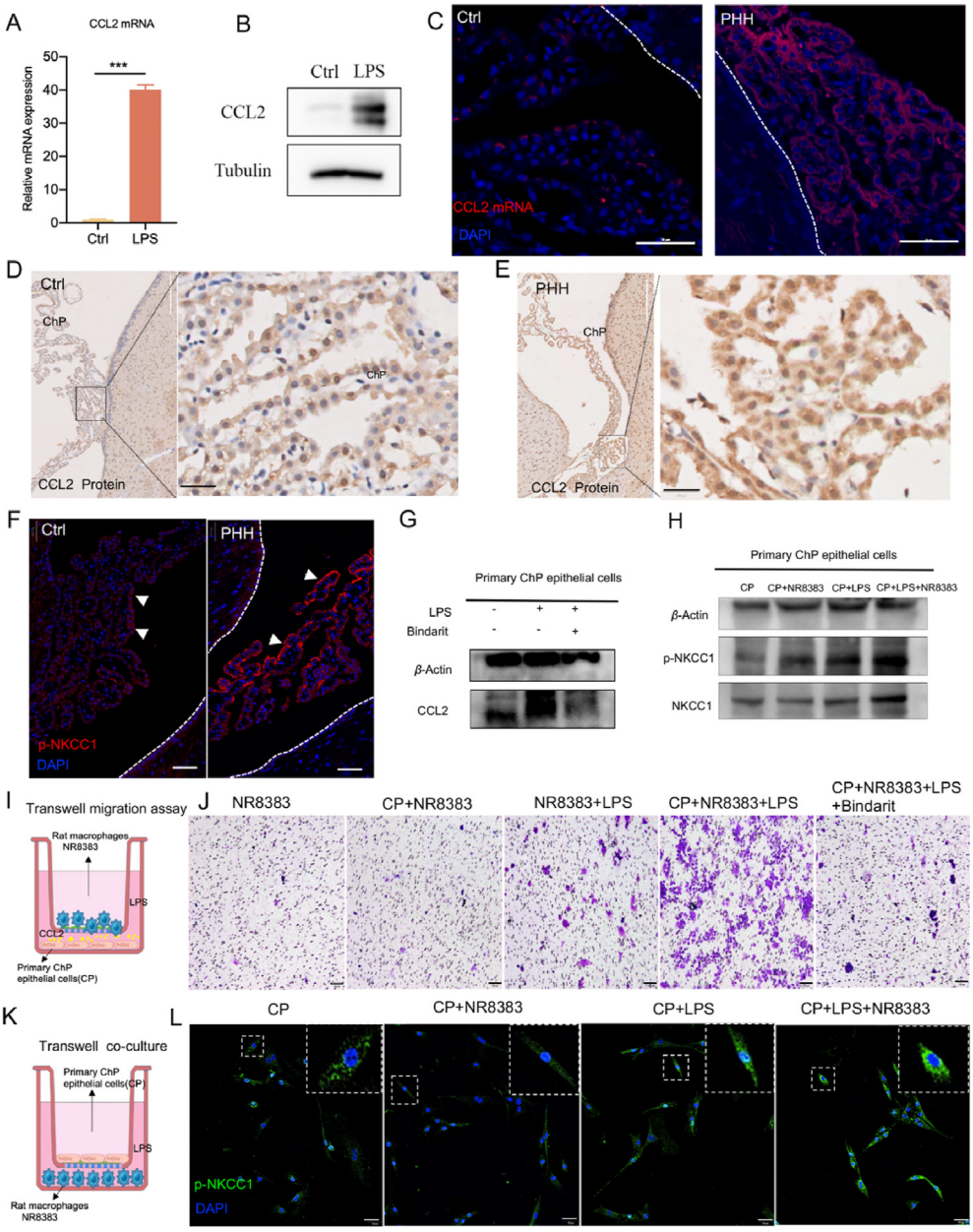

Figure 3 ChP epithelial cells contribute to CSF CCL2 and macrophages enhance the expression of p-NKCC1 in ChP epithelial cells *in vitro*. (A) Quantification of CCL2 expression in ChP epithelial cells following LPS stimulation, *via* qPCR analysis. (B) Western blot analysis illustrating CCL2 expression levels. (C) *In situ* hybridization of CCL2 mRNA exclusively expressed in ChP epithelial cells in PHH. Scale bar = 50 μm. (D, E) Immunohistochemical staining of CCL2 distribution in ChP of ctrl and PHH rats. Scale bar = 50 μm. (F) Immunofluorescence analysis of pNKCC1 (red) in ChP. Scale bar = 50 μm. (G) Western blot results of CCL2 in Bindarit-treated ChP epithelial cells. (H) Western blot analysis comparing protein profiles among different groups. (I) Schematic diagram of 2D-transwell experiment. (J) Observation of NR8383 vertical migration in the co-culture system at 24 h using transwell images. (K) A 2D-transwell system to study the effect of macrophages on ChP epithelial cells. (L) Immunofluorescence staining of pNKCC1(green) in ChP epithelial cells in different groups. All data were presented as mean ± SD, $^{*}P < 0.05$, $^{**}P < 0.01$ and $^{***}P < 0.001$ *vs.* control/model.

can initiate cellular inflammation through specific ligand-receptor interactions[33]. Consequently, we posited whether analogous mechanisms are at play in PHH. Notably, Ren et al.[34] identified TNF-α and IL-6 were the highest cytokines in supernatants collected from bone marrow-derived macrophages that were differentiated with IFN-γ/LPS. The two most prevalent and most abundant cytokines in CSF from SAH patients are the pro-inflammatory cytokines TNFα and IL-1β[35]. In addition, our study revealed a significant upregulation in TNF-α mRNA expression within the ChP following IVH. TNF-α has been well-established as an important mediator in the initiation and perpetuation of the inflammatory immune. As a result of this, we chose TNF-α as the focus of the study.

We proceeded to explore whether TNF-α, induced by macrophages, plays a central role in the inflammation of ChP epithelial cells and CSF secretion. Furthermore, Karimy et al. demonstrated

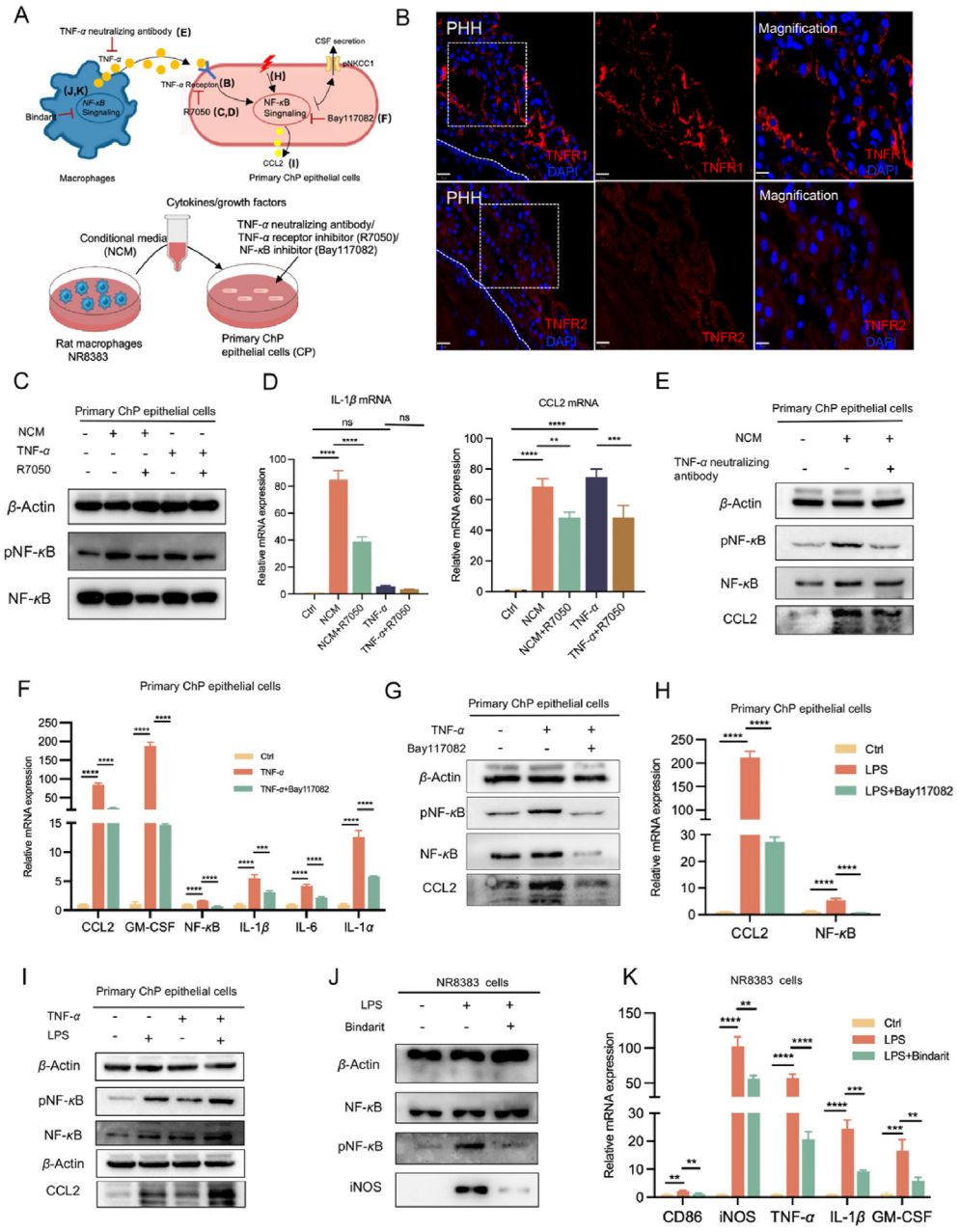

Figure 4 Macrophages enhance CSF hypersecretion in ChP epithelial cells *via* the TNF-α/TNFR1/NF-κB pathway. (A) Schematic diagram of mechanisms of crosstalk between ChP epithelial cells and macrophages. (B) Representative images showed that TNFR1 but not TNFR2 is expressed by ChP in PHH rats. Scale bar = 20 μm. (C) The expression of NF-κB and pNF-κB in ChP epithelial cells treated with NR8383 derived conditional medium (NCM), TNF-α, and R7050. (D) CCL2 and IL-1β mRNA expression in various groups. (E) The expression of NF-κB, pNF-κB, and CCL2 in epithelial cells treated with NCM or/and TNF-α neutralizing antibody. (F) The mRNA expression of proinflammatory cytokines such as CCL2, GM-CSF, IL-1β, IL-6, and IL-1α in ChP epithelial cells treated with TNF-α or/and Bay117082. (G) The expression of NF-κB, pNF-κB, and CCL2 in epithelial cells treated with TNF-α or/and Bay117082. (H) QPCR of CCL2 and NF-κB in epithelial cells treated with LPS or/and Bay117082. (I) The expression of NF-κB pathway, and CCL2 expression in ChP epithelial cells treated with LPS or/and TNF-α. (J) Western blot results of M1 marker (iNOS) and NF-κB signaling in rat macrophages NR8383 cells treated with LPS or/and Bindarit. (K) QPCR of M1 markers (iNOS and CD86) and inflammatory cytokines such as TNF-α, IL-1β, and GM-CSF in NR8383 cells treated with LPS or/and Bindarit. All data were presented as mean ± SD, $^{*}P < 0.05$, $^{**}P < 0.01$, $^{***}P < 0.001$ and $^{****}P < 0.0001$ *vs.* control/model.

that NF-κB-regulated inflammatory cytokines can enhance the activity of SPAK, pNKCC1, and several other ion channel proteins in ChP epithelial cells, leading to CSF hypersecretion; and NF-κB is itself a transcriptional regulator of SPAK and pNKCC1[3,10]. Therefore, we delved into the question of whether TNF-α induces CSF secretion by activating NF-κB signaling in epithelial cells. To address this question, we initially examined the expression of the major TNF-α receptors, namely TNFR1 and TNFR2, in primary ChP epithelial cells. The results indicated a significantly higher expression of TNFR1 mRNA compared to TNFR2 (Figs. S2G and S2H). *In vivo* fluorescence labeling coupled with confocal microscopy revealed a notable expression of TNFR1 within the ChP

of PHH rats, while TNFR2 expression was not detected (Fig. 4B). QPCR analysis further corroborated these findings by demonstrating a significantly higher level of TNFR1 mRNA compared to TNFR2 in the ChP in PHH rats (Fig. S2I). Subsequently, we collected NR8383 conditioned medium (NCM) for the treatment of primary rat ChP epithelial cells. Comparatively, in the treatment group exposed to NCM or TNF-α (10 ng/mL), there was an augmented phosphorylation of NF-κB in these epithelial cells. We also assessed the expression of proinflammatory cytokines such as IL-1β and TNF-α. Notably, the mRNA expression of these cytokines exhibited an obvious increase upon treatment with NCM and TNF-α. But the addition of TNF-α receptor inhibitor R7050 (10 μm/L) led to a significant reduction in proinflammatory cytokines and the phosphorylation of NF-κB (Fig. 4C and D, Fig. S2J and S2K). Furthermore, when TNF-α in NCM was blocked with an anti-TNF-α neutralizing antibody (5 μg/mL), it significantly inhibited the phosphorylation of NF-κB and the expression of cytokines, including CCL2 (Fig. 4E, Fig. S2L). These results indicate that the inhibition of TNF-α receptors or blocking the TNF-α effectively reduces the activation of inflammation in epithelial cells, underscoring the critical role of TNF-α in this process.

In addition, treatment with Bay117082 (a selective inhibitor of NF-κB pathway, 5 μmol/L) significantly reduced the production of proinflammatory cytokines, including CCL2, GM-CSF, IL-1β, IL-6 and IL-1α in ChP epithelial cells following TNF-α stimulation, as confirmed by QPCR (Fig. 4F). Additionally, Bay117082 effectively inhibited the phosphorylation of NF-κB, as visually depicted in Fig. 4G. Taken together, these results strongly suggest that macrophages-derived TNF-α induced inflammation and CSF secretion in epithelial cells mainly by activating TNFR1-NF-κB signaling.

Additionally, our study revealed that Bay117082 significantly inhibited LPS-enhanced CCL2 expression by suppressing the NF-κB pathway in ChP epithelial cells (Fig. 4H). We also observed a synergistic effect on ChP epithelial cell inflammation due to the combined action of TNF-α derived from macrophages and LPS. The concurrent application of LPS and TNF-α elicited a more potent response in terms of NF-κB phosphorylation and the expression of inflammatory cytokines within ChP epithelial cells, compared to their individual use (Fig. 4I, Fig. S2M). This underscores the significant role of macrophages in ChP epithelial cell inflammation. We then proceeded to investigate the potential role of Bindarit in rat macrophages and ChP epithelial cells exposed to LPS. The results depicted that Bindarit (300 μmol/L) significantly suppressed the phosphorylation of NF-κB and expression of CCL2 in ChP epithelial cells (Fig. S2D–S2F). Moreover, Bindarit exhibited a notable inhibition of M1 markers CD86 and iNOS expression, as well as NF-κB phosphorylation and the proinflammatory cytokines TNF-α, IL-1β, and GM-CSF in macrophages (Fig. 4J and K). These findings collectively suggest that Bindarit can effectively attenuate CCL2 secretion by ChP epithelial cells and impede M1 polarization in macrophages by modulating the NF-κB signaling pathway.

3.5. *Augmentation of ChP−CCL2 induces macrophage infiltration, proliferation, CSF hypersecretion, and ventriculomegaly in vivo*

To investigate the impact of sustained CCL2 production by the ChP on CSF secretion and the immune microenvironment of the ChP. We utilized AAV2/5 vectors to induce CCL2 overexpression specifically within the ChP. AAV2/5 has been proven to have tropism for epithelial cells[36]. Administration of AAV was performed *via* in-utero intracerebroventricular (ICV) injection on Day 1, followed by the injection of 200 μL autologous blood into the lateral ventricle on Day 21. On Day 23, we quantified the lateral ventricle volume using T2-weighted magnetic resonance imaging (MRI) and obtained samples immediately after that (Fig. 5A).

Firstly, we confirmed the tropism of AAV for ChP in AAV-mCherry group (Fig. 5B). QPCR demonstrated increased CCL2 expression in ChP of AAV−CCL2 group (Fig. 5C). IHC analyses demonstrated a noteworthy upregulation of CCL2 expression in the AAV−CCL2 group (Fig. 5D). Additionally, ELISA analysis revealed a significant elevation of CCL2 levels in the CSF (Supporting Information Fig. S3E). Subsequently, we found that ChP CCL2 overexpression increased CSF secretion rates in live rats and AAV−CCL2 rats exhibited a substantial increase in CSF volume, as evidenced by enlarged lateral ventricles on cranial MRI images (Fig. 5E–G).

Subsequently, we investigated the influence of CCL2 overexpression on macrophage recruitment in the ChP. AAV−CCL2 rats resulted in a significant increase of IBA1$^+$ macrophages within the ChP. The macrophage distribution shifted towards an irregular pattern and a subset of ChP IBA1$^+$ cells were positioned between the ChP epithelial cells. Additionally, the number of IBA1$^+$ macrophages in the subependymal zone increased, suggesting macrophage activation, infiltration, and migration in the ChP under sustained CCL2 stimulation (Figs. S3A and S3B). Moreover, our study has unveiled that there was a significant augmentation in the populations of CD68$^+$; IBA1$^+$ macrophages as well as Ki67$^+$ cells (Fig. 5H, Fig. S3C and S3D), in comparison to the IVH cohort. These observations underscore the potent influence of enhanced CSF−CCL2, triggered by ChP-mediated CCL2 overexpression, in promoting infiltration and proliferation of IBA1$^+$ macrophages through the ChP barrier. The expression of pNKCC1 in ChP was also increased in AAV−CCL2 rats (Fig. 5I), suggesting that ChP macrophage infiltration promoted CSF secretion. We then investigated to ascertain whether ChP CCL2 overexpression could contribute to increased CCR2$^+$ macrophage accumulation. Subsequent immunostaining depicted that AAV−CCL2 significantly increased CCR2$^+$ monocytes in ChP (Fig. 5J and K). Hence, this data supports CCL2 expression in the ChP, and CSF could recruit peripheral CCR2$^+$ monocytes to the ChP, thus triggering an inflammatory response. Our immunofluorescence analysis has also illuminated amplified TNF-α expression within the ChP, a sentiment corroborated by the ELISA assay which exhibited heightened levels of the inflammatory cytokines TNF-α and IL-1β within the CSF of the AAV−CCL2 group (Fig. S3E–S3H). These findings collectively enrich our comprehension of the intricate mechanisms governing macrophage responses to fluctuations in CSF−CCL2.

3.6. *ChP CCL2 or CCR2 deficiencies effectively mitigate macrophage infiltration, reduce ChP inflammation, and ameliorate hydrocephalus in vivo*

Based on our findings indicated an upregulation of the ChP CCL2/CCR2 axis in PHH, and overexpressing ChP CCL2 exacerbated hydrocephalus and the accumulation of IBA1$^+$ macrophages. Subsequently, we focused on Bindarit's potential role, a molecule with established *in vivo* efficacy in inhibiting CCL2 synthesis[37], in a rat model of PHH. In our study, we observed that rats treated

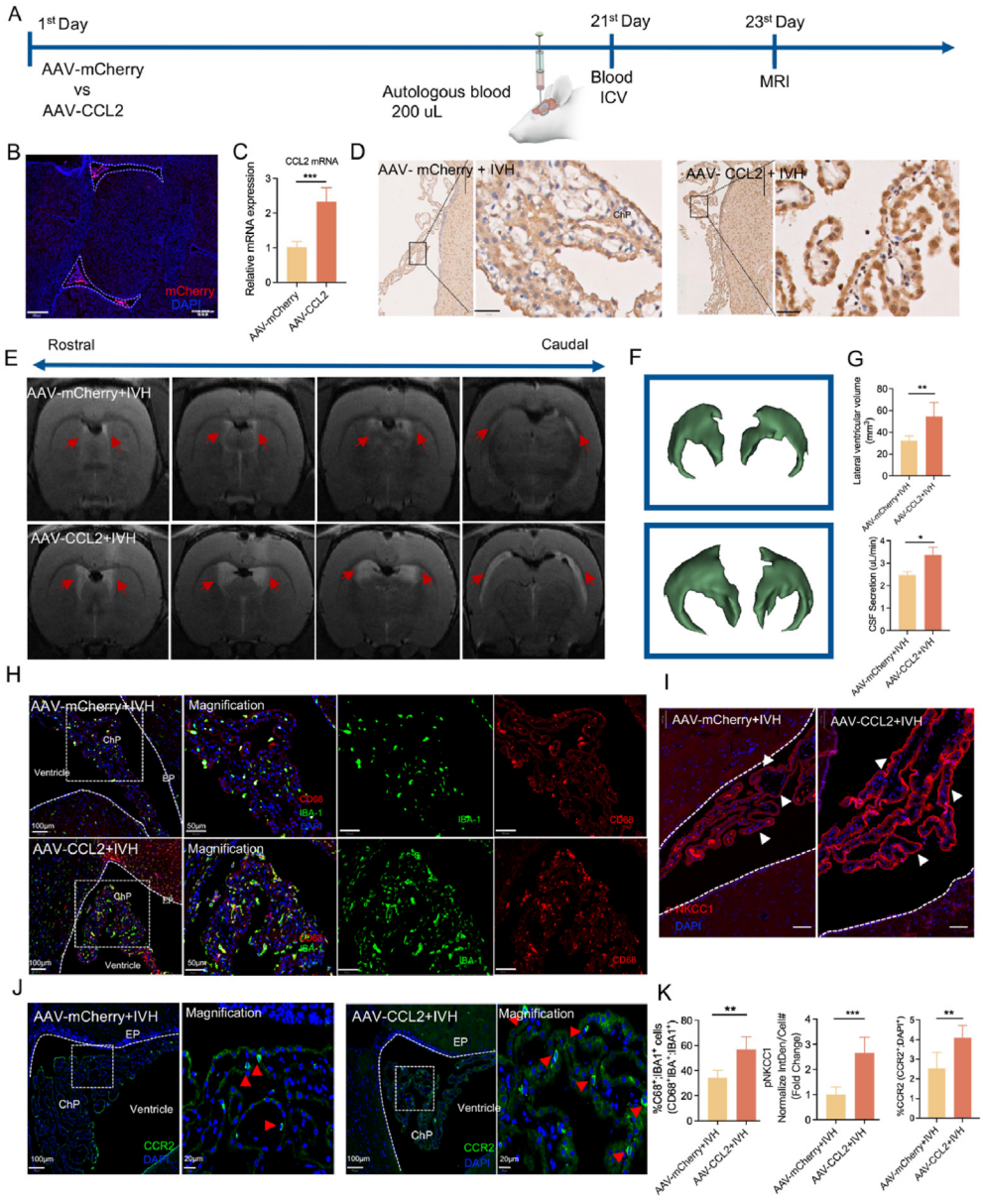

Figure 5 ChP CCL2 overexpression aggravates CSF secretion and exacerbates macrophage accumulation, activation, and CSF cytokines. (A) Schematic display of time nodes for AAV injection *in vivo*. (B) Representative image of AAV-mCherry (red) labeled brain tissue on Day 21 post-infection. (C) QPCR assessment of CCL2 expression in AAV-Cherry and AAV-CCL2 groups ($n = 5$ animals per condition). (D) Immunohistochemical staining of CCL2 expression ($n = 5$ animals per condition). (E) Representative T2-weighted MRI images of lateral ventricles in both groups ($n = 5$ animals per condition). (F) 3D reconstruction showcasing lateral ventricles. (G) Measurement of lateral ventricle volumes ($n = 5$ animals per condition) and quantification of CSF secretion rates ($n = 3$ animals per condition). (H) Increased expression of $CD68^+$(red); and $IBA1^+$ macrophages (green) in the ChP in the AAV-CCL2 group ($n = 5$ animals per condition). Scale bar = 100 μm. (I) Immunofluorescence of p-NKCC1 (red) in the ChP ($n = 5$ animals per condition). Scale bar = 50 μm. (J) The number of $CCR2^+$ macrophages (green) in ChP of AAV-mCherry and AAV-CCL2 groups ($n = 5$ animals per condition). Scale bar = 100 μm. (K) Quantitative analysis of phagocytic ChP macrophages ($CD68^+$; $Iba1^+$; % of total $Iba1^+$), p-NKCC1 expression, and % of $CCR2^+$ macrophages (green) at the ChP. All data were presented as mean ± SD, $^*P < 0.05$, $^{**}P < 0.01$ and $^{***}P < 0.001$ *vs.* control/model.

with Bindarit exhibited a marked reduction of ventriculomegaly in comparison to vehicle-treated rats (Fig. 6A and B). Furthermore, Bindarit significantly reduced the CSF secretion rate induced by IVH (Fig. 6C).

As shown in Fig. 6D, CCL2 mRNA and protein levels in the ChP and CSF were remarkably decreased by Bindarit, suggesting a successful blockage of CCL2 production. As previously evidenced, CCL2 plays a pivotal role in recruiting macrophages to the ChP. Therefore, we investigated the accumulation and activation of macrophages after Bindarit treatment. Our results indicated significant suppression of macrophage infiltration at the ChP in PHH upon Bindarit treatment (Fig. 6E and F). Additionally, there was a reduction in the number of $CD68^+$; $IBA1^+$ macrophages in the Bindarit treatment group (Fig. 6G). QPCR analysis

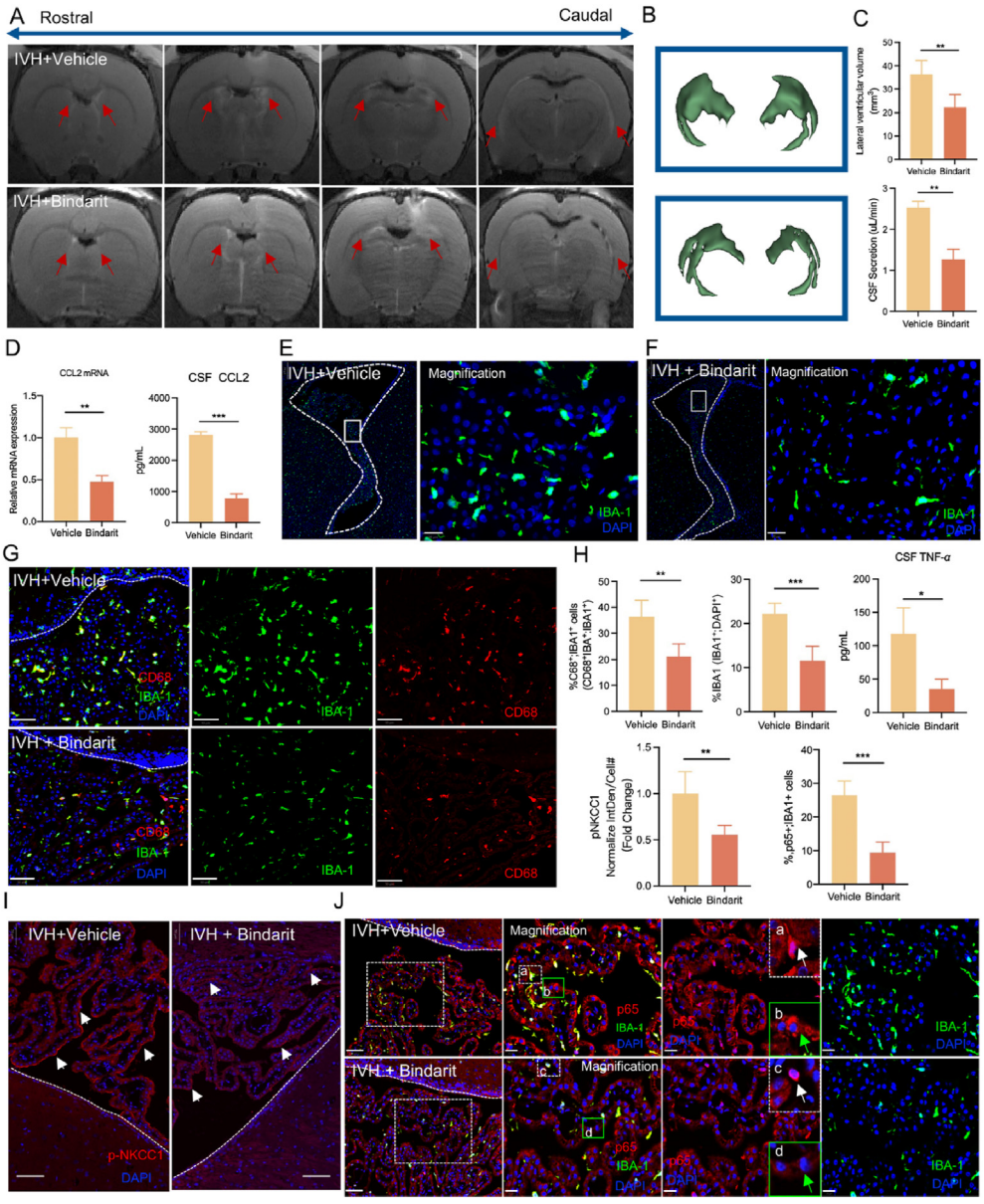

Figure 6 Knockdown of ChP CCL2 using Bindarit relieves hydrocephalus and inhibits macrophage activation. (A) Representative T2-weighted images of lateral ventricles in the PHH group and Bindarit-treated group ($n = 5$ animals per condition). (B) 3D reconstruction showcasing the lateral ventricles. (C) Quantification volumes of the lateral ventricle based on the T2-weighted images ($n = 5$ animals per condition) and evaluation of CSF secretion rates ($n = 3$ animals per condition). (D) Bindarit significantly inhibited the CCL2 mRNA expression in ChP and CSF CCL2 after Bindarit treatment ($n = 3$ animals per condition). (E, F) The number of IBA1$^+$ macrophages (green) in PHH and Bindarit-treated groups ($n = 5$ animals per condition). Scale bar = 20 μm. (G) Bindarit decreased the number of phagocytic ChP macrophages (CD68$^+$; Iba1$^+$; % of total Iba1$^+$) ($n = 5$ animals per condition), Scale bar = 50 μm. (H) Quantitative analysis of the percent of macrophages in ChP cells, % of CD68$^+$ macrophages in total macrophages, % of p65$^+$ macrophages in ChP cells, and pNKCC1 expression in ChP, as well as the expression of TNF-α in CSF. (I) Bindarit reduced the expression of p-NKCC1 (red) in the ChP. Scale bar = 50 μm ($n = 5$ animals per condition). (J) NF-κB p65 signals (red) are seen in the cytoplasm of ChP epithelial cells (green arrow, b, and d) and cytoplasm-nuclear area in macrophages (white arrow, a and c) ($n = 5$ animals per condition). Scale bar = 20 μm. All data were presented as mean ± SD, $^*P < 0.05$, $^{**}P < 0.01$ and $^{***}P < 0.001$ *vs.* control/model.

revealed the significant suppression of inflammatory genes associated with macrophage activation, including CD86 and CD40, in the Bindarit-treated ChP following IVH (Supporting Information Fig. S4A). These findings collectively suggest that the inhibition of ChP CCL2 effectively curtails macrophage infiltration, and Bindarit inhibits the proinflammatory activation of ChP macrophages. Moreover, there was a noteworthy reduction in inflammatory cytokine TNF-α within the ChP and CSF, as demonstrated by immunofluorescence (Fig. S4B−S4D) and ELISA (Fig. 6H). Most notably, the inhibition of ChP macrophages by Bindarit significantly downregulated the expression of pNKCC1 at the ChP (Fig. 6I). Additionally, Bindarit was found to suppress

IVH-induced destruction of the integrity of tight junctions between ChP epithelial cells, as evidenced in the expression of the tight junction marker ZO-1 (Fig. S4G).

Previous research has substantiated the capacity of Bindarit to attenuate the expression of inflammatory cytokines, notably CCL2, through the inhibition of NF-κB p65 phosphorylation, consequent nuclear translocation, and subsequent DNA binding[38]. In the present study, we performed immunostaining for NF-κB p65 in the ChP. In PHH, conspicuous activation of nuclear and cytoplasmic p65 signals was evident in ChP macrophages, while cytoplasmic localization of NF-κB p65 signals was observed in ChP epithelial cells. Subsequent administration of Bindarit led to a discernible reduction in the population of p65-expressing ChP macrophages. Notably, a concurrent diminishment of p65 signals in both ChP macrophages (Fig. 6J (a and c)) and epithelial cells' cytoplasmic regions (Fig. 6J (b and d)) ensued. Moreover, Bindarit treatment yielded a decrease in the nuclear p65 expression within ChP macrophages (Figs. S4E and S4F).

To further elucidate the pathological implications of CCL2/CCR2 signaling in the pathogenesis of PHH, we investigated the potential inhibitory effects of INCB 3284, a selective CCR2 antagonist that impedes CCL2 binding to CCR2[39]. The results yielded compelling results, wherein the INCB 3284 treatment regimen was associated with a pronounced reduction in ventriculomegaly, as evident in Fig. 7A–C, in stark contrast to vehicle-treated rats. Furthermore, our study revealed a notable reduction in the ChP macrophage population within the INCB 3284-treated group (Fig. 7D–F). These collective observations lend support that curtailing CCR2 activity may represent a promising avenue for mitigating hydrocephalus.

4. Discussion

Notwithstanding the common finding of neuroinflammation in hydrocephalus[40-42], the precise role of activated ChP macrophages within hydrocephalic brains remains substantially unexplored. The principal findings of the present study pertain to the central role of CCL2 signaling in the infiltration and activation of ChP macrophages, subsequently eliciting a pro-inflammatory response in hydrocephalus. The study indicates that secretion of CCL2 by ChP epithelial cells recruits CCR2$^+$ monocytes to the ChP and matures into CCR2$^+$ macrophages after IVH. The augmentation of ChP-derived CCL2 at the interface suffices to incite the activation, recruitment, and proliferation of macrophages. Suppression of either CCL2 or its receptor, CCR2, effectively mitigates the infiltration of ChP macrophages and the development of hydrocephalus after IVH. Hence, modulation of CCL2 expression or inhibition of CCR2 activity emerges as potential therapeutic modalities for ameliorating hydrocephalus. The potential of such approaches for use in human hydrocephalus remains to be explored.

Macrophages have recently emerged as the predominant class of immune cells within the ChP[31], occupying distinct niches in both the endothelial layers (referred to as stromal macrophages) and the apical epithelial surface (known as epiplexus macrophages)[43]. The ChP serves as the principal conduit for both pathogens and immune cells to access the brain, concurrently governing the presence of cytokines and various signaling molecules in the CSF[16,17]. ChP immune cell activation and recruitment into CNS have been studied in several pathological conditions including infectious diseases, autoimmune disorders, and neurodegenerative disorders[44-46]. However, the activation of ChP immune cells in PHH has received scant attention. In the present study, based on the RNA-Seq and the CIBERSORT algorithm, we have substantiated the role of monocytes and macrophages in driving ChP inflammation during PHH.

Diverse chemokines and their corresponding receptors, such as CCL2, CCL3, CCL4, CCL5, CCL7, CCL8, CCR2, and CCR5 have been implicated in orchestrating the recruitment of monocytes and macrophages in various inflammatory disorders[23,47]. Our study has unveiled that CCR2 ligands, specifically CCL2 and CCL7, are distinctly elevated within the ChP of PHH, as evidenced by the RNA-Seq dataset. Subsequent experimentation has unequivocally identified CCL2 as the most significantly upregulated chemokine. CCR2-expressing monocytes in the bloodstream are reported to routinely enter the ChP in adulthood, even in the absence of inflammatory stimuli[43]. Our investigations have highlighted that IVH triggers a marked augmentation in CCR2$^+$ macrophages within the ChP; augmented expression of ChP-derived CCL2 accentuates the accumulation of CCR2$^+$ macrophages and exacerbates hydrocephalus. Additionally, inhibiting ChP CCL2 using Bindarit significantly suppressed macrophage infiltration and hydrocephalus. In this regard, it is evident that the CCL2–CCR2 signaling cascade assumes a pivotal role in PHH, primarily through its orchestration of ChP macrophage recruitment. Notably, previous studies by Killer et al.[48] have documented heightened levels of MCP-1 protein within the CSF of hydrocephalus patients. Ziai et al.[49] observed a significant elevation of CCL2 in the CSF of individuals afflicted with intraventricular hemorrhage, and this elevation positively correlated with both the volume of intracerebral hemorrhage and perihematomal edema. In the MIA model, the embryonic ChP can recruit immune cells into CSF at the tips of ChP villi by releasing cytokines such as CCL2[50]. Furthermore, the CCL2–CCR2 axis has been reported to play an important role in several mouse inflammatory models and tumor types, by modulating monocyte recruitment[21,29,51,52]. As such, it becomes evident that CCL2, originating from the ChP and manifesting within the CSF, exerts its influence by marshaling CCR2$^+$ monocytes from the bloodstream into the ChP in PHH.

CCL2 is the most significantly increased chemokine in PHH ChP, elucidating the source of CCL2 is important to understand hydrocephalus biology and develop therapeutic interventions. In hydrocephalus, the cell types responsible for CCL2 secretion remained unclear and had never been studied. In normal ChP, epithelial cells constitute the preponderant cellular cohort, and IBA1$^+$ macrophages comprise a minority faction, constituting less than 10% of the cellular populace[3,31]. Despite this, it is known that CCL2 is predominantly secreted by immune cells in humans and mice[53,54], some studies found that other non-immune cells such as chondrocytes or synovial fibroblasts can also secrets the CCL2[23,55]. In the current study, our *in vitro* experiments depicted LPS significantly increasing the expression of CCL2 at both mRNA and protein levels in ChP epithelial cells. Furthermore, employing a two-dimensional (2D) transwell co-culture system, we cultured the rat macrophages in the upper chamber, and the primary ChP epithelial cells in the lower chamber; upon stimulation with LPS, the macrophages demonstrated a marked propensity to traverse the transwell membrane. Remarkably, upon inhibition of CCL2 secretion in ChP epithelial cells using Bindarit, the migratory capacity of macrophages exhibited a sharp decline. Based on these observations, we cannot rule out contributions by the residual ChP macrophages to overall CSF–CCL2 levels; we highlight the ChP epithelial cells are an important source of CCL2 following IVH, thereby recruiting the CCR2$^+$

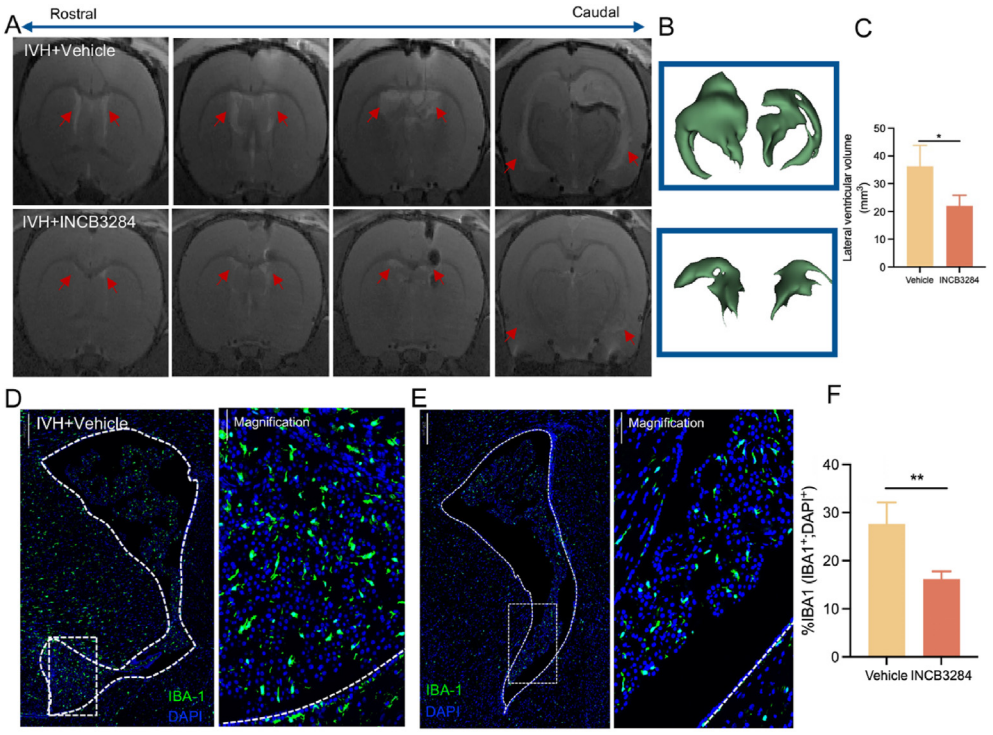

Figure 7 INCB 3284, a CCR2 inhibitor, significantly relieves hydrocephalus and macrophage infiltration. (A) Representative T2-weighted images of lateral ventricles in the PHH group and INCB 3284 treated group ($n = 3$ animals per condition). (B) 3D reconstruction showcasing lateral ventricles. (C) Lateral ventricles volume analysis. (D, E) The number of IBA1$^+$ macrophages (green) in PHH and INCB 3284 treated groups, Scale bar = 50 μm ($n = 4-5$ animals per condition). (F) Quantitative analysis of ChP macrophages. All data were presented as mean ± SD, $^*P < 0.05$, $^{**}P < 0.01$ and $^{***}P < 0.001$ *vs.* control/model.

monocytes to the ChP, which significantly increased the inflammatory cytokines and in turn leads to CSF hypersecretion.

The underlying mechanism responsible for the accumulated ChP macrophages caused CSF hypersecretion in epithelial cells and the communication between these cells remains elusive. Our results suggest ChP epithelial cells mainly expressed TNFR1 and the expression of TNFR1 increased after LPS stimulation. QPCR showed the expression of TNF-α mRNA vastly increased in ChP of PHH. Subsequently, we found that TNF-α increased phosphorylation of NF-κB, and inflammatory cytokines in epithelial cells. Meanwhile, blocking TNF-α receptors on epithelial cells and neutralizing TNF-α in the macrophages-derived conditional medium resulted in a significant reduction of inflammatory cytokines. These results suggested that the TNF-α/TNFR1 pathway might play a pro-inflammatory role in epithelial cells. Previous studies have demonstrated NK-κB mediated inflammatory cytokines play a significant role in activating SPAK, NKCC1, and several other ion channel proteins in ChP epithelial cells, leading to CSF hypersecretion[3,10]. Herein, we further examined the TNF-α/TNFR1-related intracellular pathway. The current study showed that NF-κB signaling pathways were involved in regulating TNF-α/TNFR1 signaling in ChP epithelial cells. We found that Bay117082 treatment reduced the production of proinflammatory cytokines in epithelial cells induced by TNF-α. In hydrocephalus, Karimy et al.[10] reported that NF-κB activation promoted the synthesis of proinflammatory cytokines, such as TNF-α and IL-1β in ChP epithelial cells. These cytokines, in turn, enhanced the function of SPAK and its downstream $Na^+/K^+/2Cl^-$ ion co-transporter (NKCC1); the phosphorylation of NKCC1 augments its transport capacity, leading to CSF hypersecretion by the ChP. Taken together, we concluded that TNF-α, secreted by macrophages, promotes the production of various proinflammatory factors and CSF hypersecretion in epithelial cells mainly through the TNFR1-NF-κB pathway.

In the present study, we have identified a noteworthy strategy for attenuating hydrocephalus by targeting CCL2/CCR2 signaling utilizing Bindarit and INCB3284. Bindarit is a synthetic indazole derivative molecule that can inhibit CCL2 production[29]. In *in vitro* experiments, we found that Bindarit significantly inhibited the expression of CCL2 in both rat macrophages and primary ChP epithelial cells through suppression of the NF-κB pathway. In the rat PHH model, we provided proof of concept that suppression of ChP CCL2 expression using Bindarit effectively reduced macrophage infiltration and activation, which in return restrained ChP inflammation and CSF hypersecretion. INCB3284 is a selective CCR2(hCCR2) antagonist and has been previously reported to inhibit macrophage recruiting or microglia activation in liver fibrosis and hepatic encephalopathy[56,57]. In this study, inhibition of chemokine receptor 2 (CCR2) through INCB3284 not only curtailed macrophage accumulation but also suppressed ventriculomegaly. Hence, by employing Bindarit to hinder CCL2 production and INCB3284 to selectively antagonize CCR2, we have demonstrated remarkable efficacy in diminishing macrophage infiltration and hydrocephalus, underscoring the potential therapeutic value of this dual approach. Such a treatment strategy that targets choroid plexus neuroinflammation and CSF hypersecretion may prevent shunt dependence in hydrocephalus patients. Additionally, it can also

reduce the lifelong morbidity in hydrocephalus patients and may be life-saving in regions with limited access to neurosurgical care.

5. Conclusions

Our present study demonstrates the contribution of activated ChP macrophages in the pathogenesis of hydrocephalus. Our findings robustly establish the pivotal significance of CCL2−CCR2signaling in driving ChP macrophage recruitment, activation, and proliferation in PHH. We emphasize ChP epithelial cells as a noteworthy source of CCL2 after IVH, thereby instigating the recruitment of $CCR2^{+}$ monocytes to the ChP, which significantly increases the release of inflammatory cytokines and in turn leads to CSF hypersecretion. The intricate interplay between macrophages and ChP epithelial cells plays an important role in the mechanism of CSF hypersecretion, through the TNF-α/TNFR1/NF-κB signaling cascade. Inhibition of CCL2 secretion through Bindarit significantly impedes ChP macrophage accumulation and activation, thereby mitigating ChP inflammation and ameliorating hydrocephalus. These findings underscore crosstalk between ChP epithelial cells and macrophages facilitated by CCL2−CCR2 signaling plays a vital role in CSF hypersecretion and may serve as an important therapeutic target in hydrocephalus. Additionally, we propose that Bindarit can serve as a potential treatment strategy in PHH.

Acknowledgments

We thank Huaiqiang Sun, (Animal Imaging Core Facilities, West China Hospital, Sichuan University) for MRI studies. We are grateful to the National Natural Science Foundation of China (82201501), the Natural Science Foundation of Sichuan Province (2023NSFC1581, China), and 1·3·5 projects for disciplines of excellence−Clinical Research Incubation Project, West China Hospital, Sichuan University (No. 2020HXFH013, China), and Sichuan Science and Technology Program (22ZDYF2619, China) for financial support.

Author contributions

Qiguang Wang: Conceptualization, Investigation, Writing − original draft. Fei Liu: Investigation. Yue Li: Investigation. Huan Zhang: Investigation. Xin Qi: Investigation. Ke Wu: Investigation. Yi Zhang: Investigation. Shenglan You: Investigation. Wenke Liu: Investigation. Xuhui Hui: Investigation. Hanmei Li: Writing − review & editing. Lei Zhu: Conceptualization, Writing − review & editing. Huile Gao: Conceptualization, Writing − review & editing. Jian Cheng: Conceptualization, Writing − review & editing.

Conflicts of interest

The authors have declared that no conflict of interest exists.

Appendix A. Supporting information

Supporting information to this article can be found online at https://doi.org/10.1016/j.apsb.2024.06.020.

References

1. Strahle J, Garton HJ, Maher CO, Muraszko KM, Keep RF, Xi G. Mechanisms of hydrocephalus after neonatal and adult intraventricular hemorrhage. *Transl Stroke Res* 2012;**3**:25−38.
2. Okubo S, Strahle J, Keep RF, Hua Y, Xi G. Subarachnoid hemorrhage-induced hydrocephalus in rats. *Stroke* 2013;**44**:547−50.
3. Karimy JK, Zhang J, Kurland DB, Theriault BC, Duran D, Stokum JA, et al. Inflammation-dependent cerebrospinal fluid hypersecretion by the choroid plexus epithelium in posthemorrhagic hydrocephalus. *Nat Med* 2017;**23**:997−1003.
4. Kahle KT, Kulkarni AV, Limbrick Jr DD, Warf BC. Hydrocephalus in children. *Lancet* 2016;**387**:788−99.
5. Beez T, Bellstadt L, Steiger HJ, Sarikaya-Seiwert S. Headache and shunt-related impact on activities of daily life in patients growing up with a ventriculoperitoneal shunt. *J Neurol Surg Part A* 2018;**79**:196−9.
6. Rekate HL, Kranz D. Headaches in patients with shunts. *Semin Pediatr Neurol* 2009;**16**:27−30.
7. Gupta N, Park J, Solomon C, Kranz DA, Wrensch M, Wu YW. Long-term outcomes in patients with treated childhood hydrocephalus. *J Neurosurg* 2007;**106**:334−9.
8. Steffensen AB, Oernbo EK, Stoica A, Gerkau NJ, Barbuskaite D, Tritsaris K, et al. Cotransporter-mediated water transport underlying cerebrospinal fluid formation. *Nat Commun* 2018;**9**:2167.
9. Hutton D, Fadelalla MG, Kanodia AK, Hossain-Ibrahim K. Choroid plexus and CSF: an updated review. *Br J Neurosurg* 2021:1−9.
10. Karimy JK, Reeves BC, Damisah E, Duy PQ, Antwi P, David W, et al. Inflammation in acquired hydrocephalus: pathogenic mechanisms and therapeutic targets. *Nat Rev Neurol* 2020;**16**:285−96.
11. Simard PF, Tosun C, Melnichenko L, Ivanova S, Gerzanich V, Simard JM. Inflammation of the choroid plexus and ependymal layer of the ventricle following intraventricular hemorrhage. *Transl Stroke Res* 2011;**2**:227−31.
12. Zhang Z, Tan Q, Guo P, Huang S, Jia Z, Liu X, et al. NLRP3 inflammasome-mediated choroid plexus hypersecretion contributes to hydrocephalus after intraventricular hemorrhage *via* phosphorylated NKCC1 channels. *J Neuroinflammation* 2022;**19**:163.
13. Johnsen LO, Friis KA, Damkier HH. In vitro investigation of the effect of proinflammatory cytokines on mouse choroid plexus membrane transporters Ncbe and NKCC1. *Fluids Barriers CNS* 2023;**20**:71.
14. Petitprez F, Levy S, Sun CM, Meylan M, Linhard C, Becht E, et al. The murine microenvironment cell population counter method to estimate abundance of tissue-infiltrating immune and stromal cell populations in murine samples using gene expression. *Genome Med* 2020;**12**:86.
15. Newman AM, Liu CL, Green MR, Gentles AJ, Feng W, Xu Y, et al. Robust enumeration of cell subsets from tissue expression profiles. *Nat Methods* 2015;**12**:453−7.
16. Deczkowska A, Baruch K, Schwartz M. Type I/II interferon balance in the regulation of brain physiology and pathology. *Trends Immunol* 2016;**37**:181−92.
17. Baruch K, Schwartz M. CNS-specific T cells shape brain function *via* the choroid plexus. *Brain Behav Immun* 2013;**34**:11−6.
18. Robert SM, Reeves BC, Kiziltug E, Duy PQ, Karimy JK, Mansuri MS, et al. The choroid plexus links innate immunity to CSF dysregulation in hydrocephalus. *Cell* 2023;**186**:764. 85 e21.
19. Wan Y, Hua Y, Garton HJL, Novakovic N, Keep RF, Xi G. Activation of epiplexus macrophages in hydrocephalus caused by subarachnoid hemorrhage and thrombin. *CNS Neurosci Ther* 2019;**25**:1134−41.
20. Reboldi A, Coisne C, Baumjohann D, Benvenuto F, Bottinelli D, Lira S, et al. C−C chemokine receptor 6-regulated entry of TH-17 cells into the CNS through the choroid plexus is required for the initiation of EAE. *Nat Immunol* 2009;**10**:514−23.
21. Shen Z, Kuang S, Zhang M, Huang X, Chen J, Guan M, et al. Inhibition of CCL2 by bindarit alleviates diabetes-associated periodontitis

by suppressing inflammatory monocyte infiltration and altering macrophage properties. *Cell Mol Immunol* 2021;**18**:2224−35.
22. Ben-Yehuda H, Arad M, Peralta Ramos JM, Sharon E, Castellani G, Ferrera S, et al. Key role of the CCR2−CCL2 axis in disease modification in a mouse model of tauopathy. *Mol Neurodegener* 2021;**16**:39.
23. Raghu H, Lepus CM, Wang Q, Wong HH, Lingampalli N, Oliviero F, et al. CCL2/CCR2, but not CCL5/CCR5, mediates monocyte recruitment, inflammation and cartilage destruction in osteoarthritis. *Ann Rheum Dis* 2017;**76**:914−22.
24. Baeck C, Wehr A, Karlmark KR, Heymann F, Vucur M, Gassler N, et al. Pharmacological inhibition of the chemokine CCL2 (MCP-1) diminishes liver macrophage infiltration and steatohepatitis in chronic hepatic injury. *Gut* 2012;**61**:416−26.
25. Percie du Sert N, Hurst V, Ahluwalia A, Alam S, Avey MT, Baker M, et al. The ARRIVE guidelines 2.0: updated guidelines for reporting animal research. *BMJ Open Sci* 2020;**4**:e100115.
26. Lallai V, Ahmed A, Fowler CD. Method for primary epithelial cell culture from the rat choroid plexus. *Bio Protoc* 2020;**10**:e3532.
27. Yang Y, He J, Wang Y, Wang C, Tan C, Liao J, et al. Targeting choroid plexus epithelium as a novel therapeutic strategy for hydrocephalus. *J Neuroinflammation* 2022;**19**:156.
28. Unver N. Macrophage chemoattractants secreted by cancer cells: sculptors of the tumor microenvironment and another crucial piece of the cancer secretome as a therapeutic target. *Cytokine Growth Factor Rev* 2019;**50**:13−8.
29. Georgakis MK, Bernhagen J, Heitman LH, Weber C, Dichgans M. Targeting the CCL2−CCR2 axis for atheroprotection. *Eur Heart J* 2022;**43**:1799−808.
30. Xie ST, Chen AX, Song B, Fan J, Li W, Xing Z, et al. Suppression of microglial activation and monocyte infiltration ameliorates cerebellar hemorrhage induced-brain injury and ataxia. *Brain Behav Immun* 2020;**89**:400−13.
31. Dani N, Herbst RH, McCabe C, Green GS, Kaiser K, Head JP, et al. A cellular and spatial map of the choroid plexus across brain ventricles and ages. *Cell* 2021;**184**:3056. 74.e21.
32. Liang Y, Sun X, Wang M, Lu Q, Gu M, Zhou L, et al. PP2Acalpha promotes macrophage accumulation and activation to exacerbate tubular cell death and kidney fibrosis through activating Rap1 and TNFalpha production. *Cell Death Differ* 2021;**28**:2728−44.
33. Yan Y, Merlin D. Ste20-related proline/alanine-rich kinase: a novel regulator of intestinal inflammation. *World J Gastroenterol* 2008;**14**:6115−21.
34. Ren X, Manzanares LD, Piccolo EB, Urbanczyk JM, Sullivan DP, Yalom LK, et al. Macrophage-endothelial cell crosstalk orchestrates neutrophil recruitment in inflamed mucosa. *J Clin Invest* 2023;**133**.
35. Devlin P, Ishrat T, Stanfill AG. A systematic review of inflammatory cytokine changes following aneurysmal subarachnoid hemorrhage in animal models and humans. *Transl Stroke Res* 2022;**13**:881−97.
36. Chen X, He Y, Tian Y, Wang Y, Wu Z, Lan T, et al. Different serotypes of adeno-associated virus vector- and lentivirus-mediated tropism in choroid plexus by intracerebroventricular delivery. *Hum Gene Ther* 2020;**31**:440−7.
37. Iwasawa E, Brown FN, Shula C, Kahn F, Lee SH, Berta T, et al. The anti-inflammatory agent bindarit attenuates the impairment of neural development through suppression of microglial activation in a neonatal hydrocephalus mouse model. *J Neurosci* 2022;**42**:1820−44.
38. Ling Z, Li W, Hu J, Li Y, Deng M, Zhang S, et al. Targeting CCL2-CCR4 axis suppress cell migration of head and neck squamous cell carcinoma. *Cell Death Dis* 2022;**13**:158.
39. Xue CB, Feng H, Cao G, Huang T, Glenn J, Anand R, et al. Discovery of INCB3284, a potent, selective, and orally bioavailable hCCR2 antagonist. *ACS Med Chem Lett* 2011;**2**:450−4.
40. Habiyaremye G, Morales DM, Morgan CD, McAllister JP, CreveCoeur TS, Han RH, et al. Chemokine and cytokine levels in the lumbar cerebrospinal fluid of preterm infants with post-hemorrhagic hydrocephalus. *Fluids Barriers CNS* 2017;**14**:35.
41. Schmitz T, Heep A, Groenendaal F, Huseman D, Kie S, Bartmann P, et al. Interleukin-1beta, interleukin-18, and interferon-gamma expression in the cerebrospinal fluid of premature infants with post-hemorrhagic hydrocephalus—markers of white matter damage? *Pediatr Res* 2007;**61**:722−6.
42. Holste KG, Xia F, Ye F, Keep RF, Xi G. Mechanisms of neuroinflammation in hydrocephalus after intraventricular hemorrhage: a review. *Fluids Barriers CNS* 2022;**19**:28.
43. Cui J, Xu H, Lehtinen MK. Macrophages on the margin: choroid plexus immune responses. *Trends Neurosci* 2021;**44**:864−75.
44. Mottahedin A, Joakim Ek C, Truvé K, Hagberg H, Mallard C. Choroid plexus transcriptome and ultrastructure analysis reveals a TLR2-specific chemotaxis signature and cytoskeleton remodeling in leukocyte trafficking. *Brain Behav Immun* 2019;**79**:216−27.
45. McHugh J. The choroid plexus: a cellular site of entry into the brain in NPSLE? *Nat Rev Rheumatol* 2019;**15**:452.
46. Llovera G, Benakis C, Enzmann G, Cai R, Arzberger T, Ghasemigharagoz A, et al. The choroid plexus is a key cerebral invasion route for T cells after stroke. *Acta Neuropathol* 2017;**134**:851−68.
47. Griffith JW, Sokol CL, Luster AD. Chemokines and chemokine receptors: positioning cells for host defense and immunity. *Annu Rev Immunol* 2014;**32**:659−702.
48. Killer M, Arthur A, Al-Schameri AR, Barr J, Elbert D, Ladurner G, et al. Cytokine and growth factor concentration in cerebrospinal fluid from patients with hydrocephalus following endovascular embolization of unruptured aneurysms in comparison with other types of hydrocephalus. *Neurochem Res* 2010;**35**:1652−8.
49. Ziai WC, Parry-Jones AR, Thompson CB, Sansing LH, Mullen MT, Murthy SB, et al. Early inflammatory cytokine expression in cerebrospinal fluid of patients with spontaneous intraventricular hemorrhage. *Biomolecules* 2021;**11**.
50. Cui J, Shipley FB, Shannon ML, Alturkistani O, Dani N, Webb MD, et al. Inflammation of the embryonic choroid plexus barrier following maternal immune activation. *Dev Cell* 2020;**55**:617. 28.e6.
51. Hajal C, Shin Y, Li L, Serrano JC, Jacks T, Kamm RD. The CCL2−CCR2 astrocyte-cancer cell axis in tumor extravasation at the brain. *Sci Adv* 2021;**7**.
52. Yang H, Zhang Q, Xu M, Wang L, Chen X, Feng Y, et al. CCL2−CCR2axis recruits tumor associated macrophages to induce immune evasion through PD-1 signaling in esophageal carcinogenesis. *Mol Cancer* 2020;**19**:41.
53. Dewald O, Zymek P, Winkelmann K, Koerting A, Ren G, Abou-Khamis T, et al. CCL2/monocyte chemoattractant protein-1 regulates inflammatory responses critical to healing myocardial infarcts. *Circ Res* 2005;**96**:881−9.
54. Kurihara C, Lecuona E, Wu Q, Yang W, Núñez-Santana FL, Akbarpour M, et al. Crosstalk between nonclassical monocytes and alveolar macrophages mediates transplant ischemia-reperfusion injury through classical monocyte recruitment. *JCI Insight* 2021;**6**.
55. Appleton CT, Usmani SE, Pest MA, Pitelka V, Mort JS, Beier F. Reduction in disease progression by inhibition of transforming growth factor alpha−CCL2 signaling in experimental posttraumatic osteoarthritis. *Arthritis Rheumatol* 2015;**67**:2691−701.
56. Xi SJ, Zheng XY, Li XY, Jiang YM, Wu YK, Gong J, et al. Activated hepatic stellate cells induce infiltration and formation of $CD163^{+}$ macrophages *via* CCL2/CCR2 pathway. *Front Med (Lausanne)* 2021;**8**.
57. McMillin M, Frampton G, Thompson M, Galindo C, Standeford H, Whittington E, et al. Neuronal CCL2 is upregulated during hepatic encephalopathy and contributes to microglia activation and neurological decline. *J Neuroinflamm* 2014;**11**.